ISSN 2075-1087, Gyroscopy and Navigation, 2025, Vol. 16, No.1, pp. 65-78.
Russian Text © The Author(s), 2025, published in Giroskopiya i Navigatsiya, 2025, No.1, pp. 106-124.

An Adaptive Attitude Control System for Small Satellites

A.V. Kramlikh

Samara National Research University, Samara, Russia
e-mail: kramlikh@mail.ru

Received October 4, 2024; revised December 20, 2024; accepted April 1, 2024.

Abstract: The paper describes an approach to designing an attitude control system for small spacecraft (SS), adaptive to possible failures of sensors and actuators. With this aim in view, the system loop includes its digital twin, which is de-signed to detect failures of measuring equipment using the predicted measurement values calculated based on onboard adaptive SS motion models. This approach increases the SS onboard computational burden, but prevents processing of unreliable measurement data in the feedback loop. Compensation for the failure of sensors and actuators is performed by reconfiguring the algorithmic support used to determine the SS attitude. To compensate for failures of actuators' individual channels, an algorithm for SS attitude control is pro-posed, the structure of which has the form of even Fourier series.

Keywords: small spacecraft, digital twin, control, reorientation, failure.

1. INTRODUCTION

One of the main trends in global astronautics is using nanosatellites – SS whose mass does not exceed 10 kg – to solve a wide range of research and applied problems both in near-Earth and in deep space. Currently, nanosatellites of the CubeSat standard continue to gain popularity [1, 2]. CubeSats, which were originally intended for educational purposes, also served as platforms for testing new technologies that could be developed and implemented within one or two years [1–3]. However, advances in microelectronics enabled soon enough their use in low-cost scientific missions.

According to the Nanosats Database – the World's largest database of nanosatellites [4], as of December 31, 2024, 89 countries had created and launched 2806 nanosatellites (of which 2596 were CubeSats), including 18 interplanetary ones. Russia accounts for 172 nanosatellites launched into orbit. According to forecasts [4], by the end of 2029, more than 1900 nanosatellites are planned to be launched worldwide. Along with this, the requirements for their active operation time are increasing. At the same time, nanosatellites themselves are becoming more complicated so that the inclusion of deployable structures, such as solar arrays, large antennas, propulsion systems. etc., entails the need to increase the fault tolerance of the SS onboard support systems with strict restrictions on mass, dimensions and energy consumption as well as taking into account the significant influence of external disturbances on angular motion.

To perform most scientific and applied research in space, for example, to study geophysical fields (the Earth's magnetosphere and ionosphere), it is necessary to ensure the required attitude of the SS in space. In this case, unlike missions on remote sensing of the Earth, the error in determining the orientation of the sensitivity axes of scientific equipment can reach several degrees (a value not exceeding 5 deg is considered acceptable). This problem can be solved with the help of the SS attitude control system (ACS), including a unit of sensors and actuators. The typical sensors that are conventionally used on board SS are the following [5–8]: magnetometers, luminance sensors, Sun sensors, angular rate sensors (ARS), local vertical reference sensors and, less of-ten, star trackers. Among the actuators, the most widely used are magnetic coils, flywheels, and attitude control engines [9–11].

Studies [12–14] have shown that the main reason for failures of spacecraft target missions is the failure of the onboard ACS, which may be due to failure of sensors, actuators, or the onboard ACS controller. To improve the reliability of spacecraft flights, it is necessary to ensure onboard detection of defects and compensate for failures.

The available approaches to fault detection and diagnostics are divided into two groups [15] (Fig. 1): those based on models [16–22] and on a database [23–27]. In the first case, filtering theory (Kalman filter (KF) and its modifications) [16, 17], H_∞ controllers [18], observers [19–21], and sliding control [22] are used. The second group relies on such methods as support vector machines (SVM) [23], neural networks

[24], statistical sequential analysis [25], independent component analysis [26], and the kernel-based fuzzy C-means [27]. More details about each approach can be found, for example, in [16–27].

The fault tolerance of the spacecraft ACS can be increased due to redundancy – hardware, software, information, etc., which allows for the ACS reconfiguration in the event of any malfunction on board the spacecraft. In the event of failure of actuators, the procedure consists in redistributing control to fault-free equipment in order to create the specified control torques and maintain acceptable quality of control [28].

If the ACS actuators do not provide for redundancy and there is no pre-programmed control algorithm to redistribute the functions of failed units to fault-free ones, the spacecraft controllability can be maintained by switching-over to the 'safe' mode [15, 29]. Once a malfunction is detected in the space-craft, its onboard computer disables all actuators, resulting in the suspension of the scientific experiment cyclogram until the flight control center (FCC) experts have resolved the identified problem. Thus, the 'safe' mode is uncontrolled motion of spacecraft with a minimum sufficient set of support systems. It is worth noting that the fact of abnormal functioning of the spacecraft is actually recognized by the FCC experts based on the telemetry analysis. This is basically the only approach used to eliminate emergency situations on board a spacecraft [15]; its effectiveness was demonstrated on the example of the FUSE (Far Ultraviolet Spectroscopic Explorer) [15, 30] and the CERISE spacecraft [15, 31].

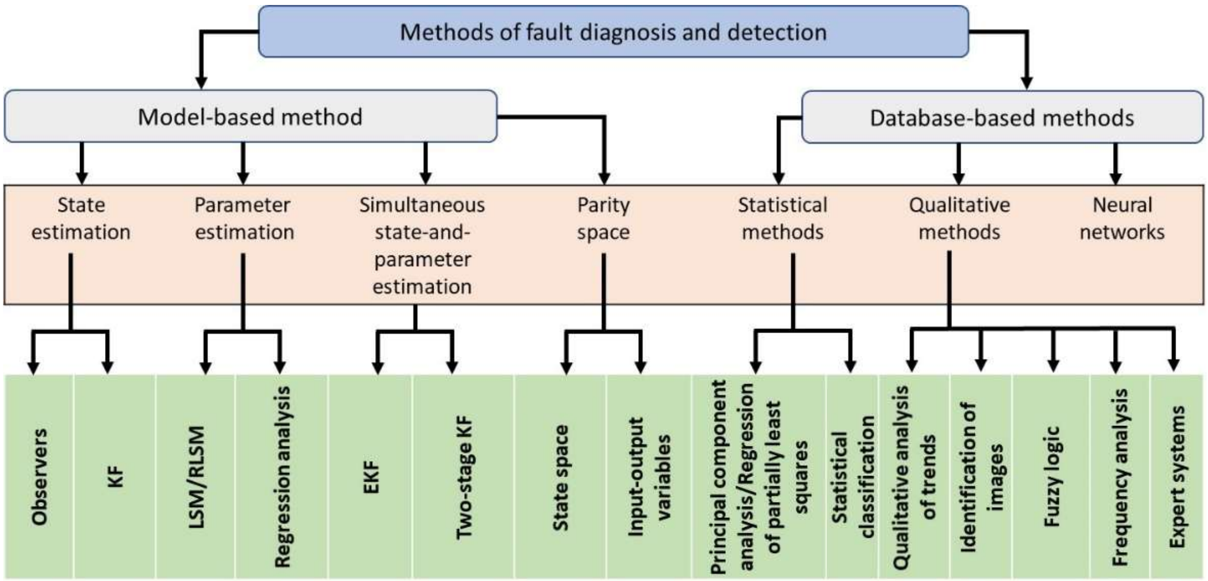

Fig. 1. Classification of ACS fault diagnosis and detection methods (KF – Kalman filter, LSM – least square method, RLSM – recurrent LSM, EKF – extended Kalman filter).

Due to strict restrictions on SS mass and dimensions, it is difficult to ensure redundancy of the ACS actuators. At the same time, with long communication delays, in particular during interplanetary missions or during short-term communication sessions, or complication of scientific research, the 'safe' mode may prove to be ineffective. In this regard, it seems relevant to create adaptive autonomous systems for detecting and compensation for failures of SS sensors and actuators (without redundancy of actuators), which can be built on the basis of modern energy-efficient onboard computing facilities.

In this connection, the author proposes a new approach to designing an ACS for SS, the one that can adapt to possible failures of sensors and actuators.

The article is structured as follows. Section 2, following Introduction, de-scribes the SS ACS adaptation to possible faults. Section 3 presents the mathematical models of motion and measurements used in the ACS digital twin. Section 4 discusses the methodology used to detect failures of measuring equipment, also considered are the mathematical models implemented in the ACS digital twin. Sections 5 and 6 present the solutions to the problems of designing a fault-tolerant SS ACS – synthesis of nominal control of SS reorientation in the event of failure of one or two control channels.

2. ADAPTATION OF THE SS ATTITUDE CONTROL SYSTEM TO POSSIBLE FAILURES

In order to increase the SS ACS fault tolerance in the missions where it is of critical importance, we propose its adaptive modification based on the parallel operation of the SS ACS and its digital twin. In the event of detection of faults in the measuring or actuator devices in the digital twin, a decision is generated to reconfigure the algorithmic support of the SS ACS (Fig. 2).

The task of designing a fault-adaptive SS ACS includes two parts:

• design of a fault-tolerant feedback loop for the control system – determining the SS attitude in the case that one or more measuring devices fail;

• design of a fault-tolerant forward loop for the control system – maintaining controllability in the event of failure of individual actuators.

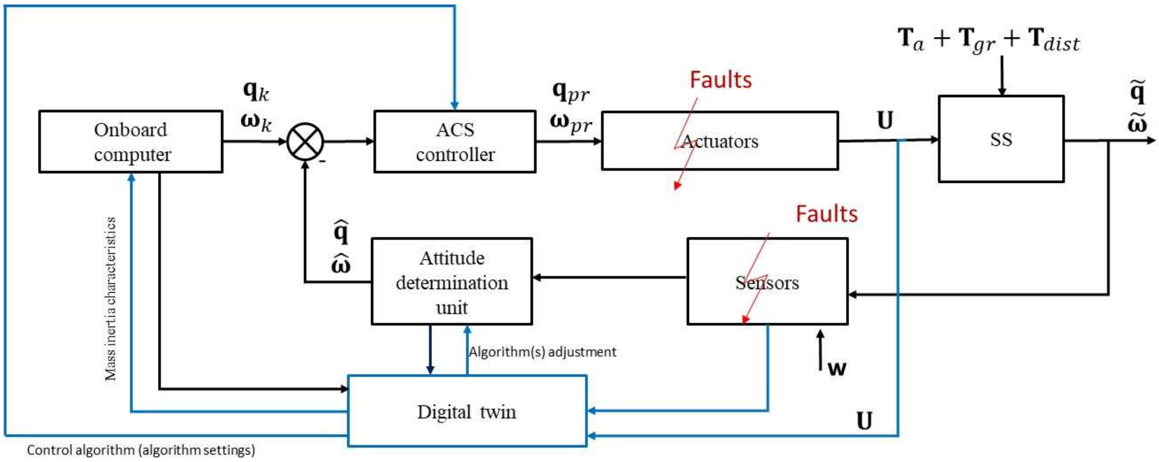

Fig. 2. Schematic of the SS angular motion control circuit with a digital twin.

3. DIGITAL TWIN OF THE SS ATTITUDE CONTROL SYSTEM

In accordance with [32], a digital twin of a product is a system consisting of its digital model and two-way information links with it (if any) and/or its component parts.

In this case, the digital twin of the ACS is a set of mathematical models and algorithms for determining SS attitude and controlling its angular motion, its main tasks being as follows:

- modeling of the SS center-of-mass motion;
- modeling of the SS uncontrolled angular motion;
- modeling of the SS onboard sensors' measurements;
- calibration of measuring devices;
- identification of the SS onboard model parameters;
- modeling of the algorithms performance for determining SS attitude;
- modeling of the SS controlled angular motion.

The diagram of interaction between models and algorithms in the ACS digital twin is shown in Fig. 3.

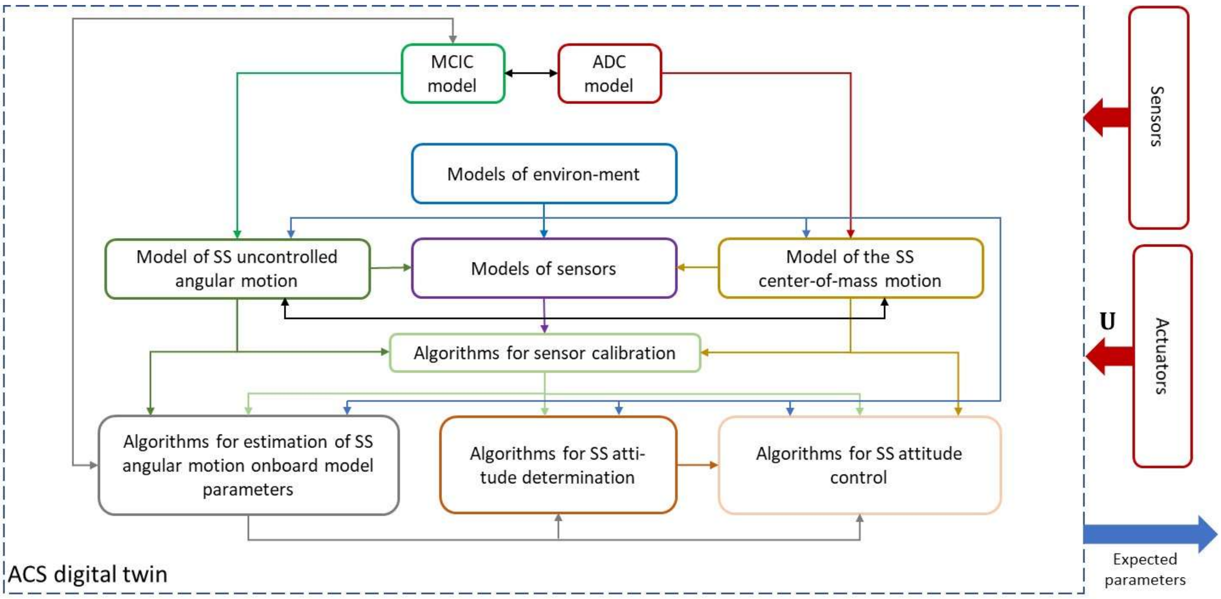

Fig. 3. A diagram of interaction between models and algorithms in the ACS digital twin (MCIC – mass centering and inertia characteristics (mass, center-of-mass position, inertia tensor); ADC – aerodynamical characteristics (center-of-pressure position, drag coefficient).

Let us describe the main reference frames used in the digital twin.

The absolute Earth-centered earth-fixed (ECEF) reference frame (*e*-frame) $ox_ay_az_a$: the origin *o* is in the center of the Earth; axis ox_a is directed to the vernal equinox point, axis oz_a – along the axis of the Earth's daily rotation (perpendicular to the equatorial plane), axis oy_a lying in the Earth's equatorial plane complements it to the right one (Fig. 4).

The orbital coordinate frame *OXYZ* (*o*-frame): the origin *O* is in the SS center of mass; axis *OZ* is directed along the SS radius vector; axis *OX* is perpendicular to axis *OZ*, it belongs to the SS plane of motion and is aligned with of the SS motion; axis *OY* complements the *OXYZ* to the right-hand rectangular frame (Fig. 4).

Body-fixed frame *Oxyz* (*b*-frame): the origin *O* is in the SS center of mass; the axes are aligned with the principal central axes of inertia (Fig. 5).

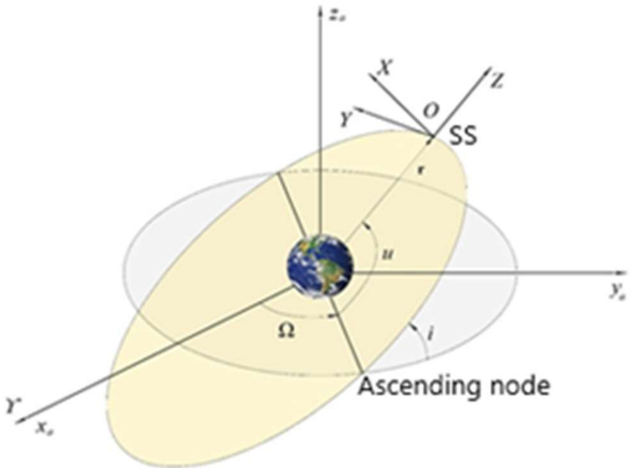

Fig. 4. Absolute and orbital coordinate frames (Ω – longitude of the ascending node, *i* – orbit inclination, *u* – argument of latitude)

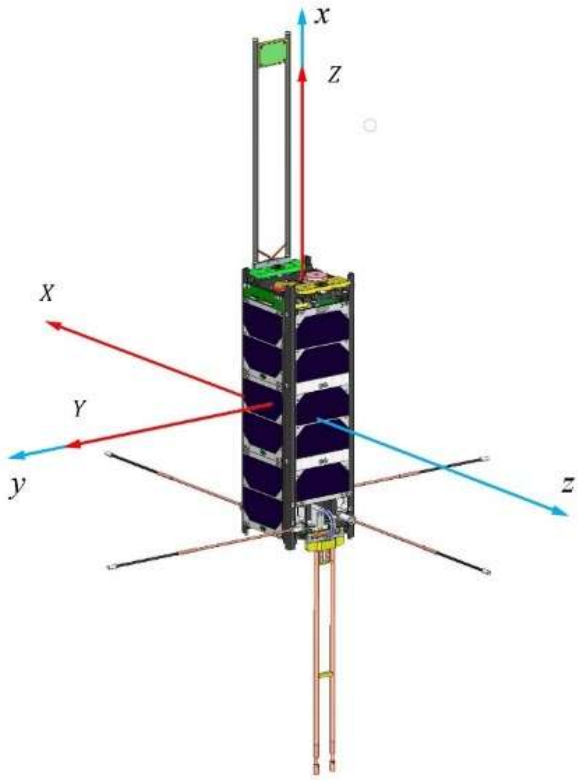

Fig. 5. Directions of the body-fixed coordinate system

Consider the main models of the digital twin.

The model of the SS center-of-mass motion in the e-frame. The SS attitude in orbit is specified by the radius vector $\mathbf{r} = [x_a \quad y_a \quad z_a]^{\mathrm{T}}$ from the center of the Earth to the SS center of mass. The equations of the center-of-mass motion in vector form have the following form [33]:

$$\ddot{\mathbf{r}} = -\mu \frac{\mathbf{r}}{|\mathbf{r}|^3} + \sum_{k=1}^{6} \delta\ddot{\mathbf{r}}_{J_k} + \delta\ddot{\mathbf{r}}_{atm}, \tag{1}$$

where μ = 398 600 is the Earth's gravitational parameter, $\mathrm{km}^3/\mathrm{s}^2$;

$\delta\ddot{\mathbf{r}}_{J_k}$ is disturbing acceleration from the *k*-th zonal harmonic;

$\delta\ddot{\mathbf{r}}_{atm}$ is disturbing acceleration from the atmospheric drag.

The equations of the SS spatial motion relative to the center of mass under the action of aerodynamic, gravitational, and control torques in a circular orbit can be written as follows:

$$\mathbf{I}\dot{\boldsymbol{\omega}} + \boldsymbol{\omega} \times \mathbf{I}\boldsymbol{\omega} = \mathbf{T}_a + \mathbf{T}_{gr} + \mathbf{U}, \tag{2}$$

where $\mathbf{I} - diag(I_x, I_y, I_z)$ is the SS tensor of inertia;

$\boldsymbol{\omega} = \boldsymbol{\omega}^{bo} + \boldsymbol{\omega}^{oa}$ is the vector of the absolute angular rate;

$\boldsymbol{\omega}^{bo} = [\omega_x^{bo}, \omega_y^{bo}, \omega_z^{bo}]^{\mathrm{T}}$ is the vector of the SS angular rate relative to the *o*-frame; $\boldsymbol{\omega}^{oa} = \left[0, \sqrt{\frac{\mu}{|\mathbf{r}|^3}}, 0\right]^{\mathrm{T}}$ is the *o*-frame angular rate relative to the *e*-frame; $\mathbf{T}_a = \rho C_D S [\mathbf{d} \times \mathbf{V}^b] |\mathbf{V}^b|$ is the vector of the aerodynamic torque; $\mathbf{T}_{gr} = \frac{3\mu}{|\mathbf{r}|^3}\left(\boldsymbol{\eta}^b \times \mathbf{I}\boldsymbol{\eta}^b\right)$ is the vector of the gravitational torque;

$\mathbf{U} = \left[u_x, u_y, u_z\right]^{\mathrm{T}}$ is the vector of the actuators' control torque;

$\boldsymbol{\eta}^b$ is the vector of the local vertical in the b-frame;

ρ is atmospheric density at the SS altitude;

C_D is the drag coefficient;

d is the vector connecting the center of mass and the center of pressure**;**

$\mathbf{V}^b$ is the SS orbital velocity vector in projections on the b-frame.

In [34] it is shown that the SS angular acceleration due to the aerodynamic torque is significantly higher than that of spacecraft with larger dimensions and mass (with the same values of the relative static stability margin and bulk density). In this regard, to improve the accuracy of the aerodynamic torque specification it is proposed to use NRLMSISE-00 empirical model of the atmosphere [35], since in this case, its density is calculated taking into account the concentration of gases (molecular nitrogen and oxygen, atomic nitrogen and oxygen, helium, hydrogen, and argon), which depends on the SS space-time position, the Sun activity, and the current state of the Earth's magnetic field. The error in determining the SS aerodynamic characteristics can be reduced using the panel method [36] or the direct simulation Monte Carlo method [37], which make it possible to obtain the drag coefficients, lift and lateral forces, as well as the center-of-pressure coordinates, taking into account both the diffuse interaction of particles with the surface and their thermal velocities.

Let us complement the dynamic equations (2) with a kinematic one in vector form with a normalized quaternion:

$$\dot{\mathbf{q}} = \frac{1}{2}\boldsymbol{\Omega}\mathbf{q}, \tag{3}$$

where $\mathbf{q}$ is a normalized quaternion; $\boldsymbol{\Omega} = \begin{bmatrix} 0 & -\omega_x^{bo} & -\omega_y^{bo} & -\omega_z^{bo} \\ \omega_x^{bo} & 0 & \omega_z^{bo} & -\omega_y^{bo} \\ \omega_y^{bo} & -\omega_z^{bo} & 0 & \omega_x^{bo} \\ \omega_z^{bo} & \omega_y^{bo} & -\omega_x^{bo} & 0 \end{bmatrix}$ is a skew-symmetric matrix.

The mathematical model of magnetometer measurements can be represented as [38]

$$\mathbf{B}_m = \mathbf{S}\cdot\mathbf{N}\cdot\left(\mathbf{A}_{si}\cdot\mathbf{B}_t + \mathbf{b}_{hi}\right) + \mathbf{b}_{so} + \boldsymbol{\beta}(t) + \boldsymbol{\varepsilon}, \tag{4}$$

where $\mathbf{B}_t$ is a true value of the induction vector of the measured Earth's external magnetic field; $\mathbf{B}_m$ is the vector of magnetometer measurements; $\mathbf{A}_{si}$ is a matrix of the error caused by soft magnetic materials; $\mathbf{b}_{hi}$ is the vector of zero bias caused by hard magnetic materials; $\mathbf{N}$ is a matrix of the magnetometer axes nonorthogonality; $\mathbf{S}$ is a diagonal matrix of scaling along the magnetometer measuring axes; $\mathbf{b}_{so}$ is the vector of instrumental zero bias; $\boldsymbol{\beta}(t)$ is the vector of temperature zero bias, the components of which change over time and depend on the ambient temperature; $\boldsymbol{\varepsilon}$ is the vector of measurement noise, the components of which are random variables with a normal distribution law and zero mathematical expectation.

To model measurements $\mathbf{B}_t$, we used the well-known model of the Earth's magnetic field (EMF) – the International Geomagnetic Reference Field (IGRF) developed by the International Association of Geomagnetism and Aeronomy (IAGA). The model is a set of coefficients of the Earth's magnetic potential expansion in a series of spherical functions. It contains coefficients not only for the year of the epoch (updated every five years), but also taking into account secular changes [6]. In practice, 13 harmonics of the Earth's magnetic potential expansion are most often used.

The mathematical model of ARS measurements can be represented as [39]

$$\boldsymbol{\omega} = \boldsymbol{\omega}_t + \mathbf{N}_\omega\boldsymbol{\omega}_t + \mathbf{S}_\omega\boldsymbol{\omega}_t + \mathbf{b}_\omega + \boldsymbol{\varepsilon}, \tag{5}$$

where $\boldsymbol{\omega}$ is the vector of ARS measurements; $\boldsymbol{\omega}_t$ is the vector of the sensitivity axis the elements of which are the projections of the acting true angular rate; $\mathbf{b}_\omega$ is the vector whose elements are the zero-bias errors for each sensitivity axis; $\mathbf{S}_\omega$ is the scale-factor error matrix; $\mathbf{N}_\omega$ is the matrix of ARS axes nonorthogonality errors; $\boldsymbol{\varepsilon}$ is the vector of random measurement noise, the components of which are random variables with a normal distribution law and zero mathematical expectation.

The modeling of ω_t measurements is performed using Eqs. (2)–(3).

The Sun sensor measures the Sun direction vector in the b-frame [8], and the measurement model has the form [40]:

$$\mathbf{S}_b = \mathbf{A}\mathbf{S}_r + \boldsymbol{\varepsilon}, \tag{6}$$

where $\mathbf{S}_r$ is the vector of direction to the Sun in the base reference frame (for example, o-frame); $\mathbf{A}$ is the transition matrix from the base reference frame to the b-frame; $\boldsymbol{\varepsilon}$ is the vector of random measurement noise, the components of which are random variables with a normal distribution law and zero mathematical expectation.

To simulate $\mathbf{S_r}$ measurements, we use the VSOP (Variations Séculaires des Orbites Planètaires) planetary motion model – a set of coefficients for calculation of the heliocentric coordinates of the planets [41].

4. METHODOLOGY FOR DETECTING FAILURES OF MEASURING EQUIPMENT

The method for detecting failures of measuring sensors and actuators is based on mathematical models of motion (1)–(3) and measurements (4)–(6), which are implemented in the digital twin.

To compensate for the effects of space factors on the sensitive elements of the measuring instruments of the SS ACS, such as zero bias, it is necessary to periodically calibrate them [8, 42, 43]. The procedure for diagnosing failures of measuring equipment consists of several stages.

Stage 1. Identification of the SS parameters (onboard motion model — mass, inertia tensor) based on the results obtained in processing the measurements made at the previous stage of the flight [44]. This stage is performed if the SS is equipped with transformable elements or a propulsion system.

Stage 2. Prediction of the SS center-of-mass motion parameters according to Eqs. (1) and the SS angular motion according to Eqs. (2)–(3) at the required moment in time.

Stage 3. Calculation by appropriate models of vector measurement in the *o*-frame.

Stage 4. Recalculation of the models of vector measurement from the *o*-frame to the *b*-frame; the result obtained will be called the calculated measurement.

Stage 5. Calculation of the value of δ as the difference between the calculated and measured values. If δ does not exceed δ_{lim}, the measurements are used in the control loop, otherwise the algorithm for determining the SS attitude is reconfigured.

The value of δ_{lim} is specified for each type of measurements taking into account the level of their noise based on the results of ground tests (ground calibration) or is calculated in flight. If ground tests cannot be carried out, nominal (passport) values are taken.

5. DESIGN OF THE FAULT-TOLERANT FEEDBACK LOOP OF THE SS ATTITUDE CONTROL SYSTEM

The SS ACS feedback loop is designed to determine the current attitude and angular rate based on the information from the SS measuring equipment, which may include magnetometers, ARS, Sun sensors, a GNSS receiver (information on the geometric visibility of navigation spacecraft (NSC)).

The SS attitude is calculated using a set of algorithms both based on single-moment measurements [6, 8, 40] and on the Kalman filter [6, 8, 40, 45, 46]. The algorithm is selected based on the results obtained at Stage 5 of the diagnostic procedure. When the SS is operating in the normal mode, it is assumed that the attitude determination problem is solved in two stages [45–47]. First, the magnetometer and Sun sensor measurements are processed, for example, by the QUEST algorithm [8], SVD [8], or any other similar algorithm, the output of which is a normalized quaternion, which in turn is a priori information for the Kalman filter input (second stage). It is here that the measurements from the magnetometer and ARS arrive.

If an ARS fails, the approach to the problem solution remains equivalent to that in the standard mode, except that only magnetometer measurements are used in the Kalman filter [45, 47].

In the case of a Sun sensor failure, information from the GNSS on the NSC geometric visibility is added to the magnetometer readings in the algorithm for single-moment measurements, and then the standard operation scheme is activated.

If a magnetometer fails, the algorithm for single-moment measurements uses information from the Sun sensor and the geometric visibility of the NSC; the Kalman filter works only with the ARS data.

If magnetometers and an ARS are damaged, the attitude determination problem is solved during the operating time of the GNSS receiver (its continuous operation is not considered) due to the algorithms that use information on the NSC geometric visibility [48].

If there is at least one normally functioning vector sensor on board the spacecraft, its orientation can be determined by processing the accumulated sample of measurements [49, 50].

6. DESIGN OF THE FAULT-TOLERANT DIRECT LOOP OF THE SS ATTITUDE CONTROL SYSTEM

In [51], the authors studied the influence of the control form represented by the power and trigonometric series, odd and even Fourier series, as well as the Schlömilch series, on the minimum value of the objective function in order to solve the terminal problem of SS angular motion control. Of the series considered, the best, i.e. minimum, value of the objective function is provided by the even Fourier series, which proved to be efficient in solving the above-mentioned problem in the case of failure of one control channel [52]. Both for the terminal problem and in the case of failure of one channel, the search for the control function is reduced to multiparameter optimization.

The terminal problem of SS angular motion control is formulated as follows: the SS whose angular motion is described by Eqs. (2)–(3) must be moved from a certain arbitrary initial position

$$\mathbf{q}\big|_{t=0} = \mathbf{q}_0, \boldsymbol{\omega}\big|_{t=0} = \boldsymbol{\omega}_0 \tag{7a}$$

to a required position

$$\mathbf{q}\big|_{t=t_\kappa} = \mathbf{q}_k, \boldsymbol{\omega}\big|_{t=t_\kappa} = \boldsymbol{\omega}_\kappa \tag{7b}$$

within a fixed time interval t_k.

Reorientation of the spacecraft with a failed control channel is carried out using the following structure of control (for each of the nonfailed channels):

$$U(t) = \frac{a_0}{2} + \sum_{n=1}^{8} a_n \cos\left(\frac{2\pi n t}{t_k} + \theta_n\right), \tag{8}$$

where a_0, a_n, θ_n are unknown parameters to be determined.

If one control channel fails, 34 unknown parameters are to be found (9 coefficients a_n and 8 coefficients θ_n for each operating channel) or 17 (in the case that two channels have failed). The search for unknown parameters a_0, a_n, θ_n was performed by zero-order optimization—the differential evolution algorithm [53].

Finding the unknown coefficients a_0, a_n, θ_n of control (8) is reduced to minimization of the objective function of the form:

$$f(\mathbf{a}, t_k) = \\ = \arccos\left[\frac{1}{2}\left(\mathrm{tr}\left(\mathbf{A}^{\mathrm{T}}(\mathbf{q}_k)\mathbf{A}^{\mathrm{T}}\left(\mathbf{q}_k^{real}\right)\right) - 1\right)\right] + t_k\left|\boldsymbol{\omega}_k - \boldsymbol{\omega}(t_k)\right|, \tag{9}$$

where $\mathbf{a} = [a_0, a_n, \theta_n]^{\mathrm{T}}$ is the vector of the parameters being estimated; $\mathbf{A}(\mathbf{q}_k)$ is the matrix of transition from the o-frame to the b-frame calculated using the required normalized quaternion (7b); $\mathbf{A}\left(\mathbf{q}_k^{real}\right)$ is a matrix of transition from the o-frame to the b-frame calculated using the real normalized quaternion.

The criterion for terminating the search for the minimum of the target function (9) is

$$\Delta = \left|f_j - f_{j-1}\right| < 10^{-4},$$

where j is the iteration number; the value of the criterion $\Delta = 10^{-4}$ was determined from the simulation results based on the convergence of the solution to problem (9).

As an example, consider a model problem for an SS with the characteristics given in Table 1. The SS orbital altitude is H = 550 km.

Table 1. SS characteristics

Parameter	Value
Inertia tensor, kgm^2	$\mathbf{I} = \begin{bmatrix} 0.0138 & 0 & 0 \\ 0 & 0.0729 & 0 \\ 0 & 0 & 0.0714 \end{bmatrix}$
Midsection S, m^2	0.01
Static stability margin Δx, m	0.06

Table 2 presents the numerical values of the boundary conditions given by (7a)–(7b).

Reorientation time, $t_k = 7100$ s.

Table 2. Boundary conditions for the model problem

Parameter	Initial conditions	Final conditions
Angular rate vector **ω**, deg/s	$[0.1\ \ 0.1\ \ 0.1]^{\mathrm{T}}$	$[0\ \ 0\ \ 0]^{\mathrm{T}}$
Orientation vector (Euler angles), deg	$[60\ \ 70\ \ 30]^{\mathrm{T}}$	$[1\ \ 1\ \ 179]^{\mathrm{T}}$
Orientation vector (quaternion)	$[0.579\ \ 0.579\ \ 0.554\ \ 0.1485]^{\mathrm{T}}$	$[0\ \ 1\ \ 0\ \ 0]^{\mathrm{T}}$

Figures 6–9 show the plots obtained during the solution of SS reorientation problem (7) according to the nominal program (8) with one failed control channel.

In the case of failure of the channel along the Ox-axis, the values of the angular rate components during the reorientation process did not exceed 2 deg/s (see Fig. 7), and the control torque along the remaining channels was $1.5 \cdot 10^{-6}$ Nm (see Fig. 6).

In the case of failure of the channel along the Oz-axis, the SS behaves in the same way as in the case of failure of the Oy channel, which is explained by the proximity of the moments of inertia. As can be seen from the figures, the angular rate components during the reorientation process did not exceed 6 deg/s (see Fig. 9), which is acceptable, and the value of the control torque along the remaining channels was no more than $3 \cdot 10^{-6}$ Nm (see Fig. 8). This is feasible for magnetic actuators, which are most often used in CubeSats.

The total error in solving the reorientation problem is usually calculated in accordance with [54]:

$$\delta = \arccos\left[\frac{1}{2}\left(\operatorname{trace}\left(\mathbf{A}^{\mathrm{T}}(\mathbf{q}_k)\mathbf{A}^{\mathrm{T}}\left(\mathbf{q}_k^{real}\right)\right)-1\right)\right], \quad (10)$$

and the error in angular rate will be judged by the difference in modulus:

$$\Delta\omega_j = \left|\omega_{jk} - \omega_j(t_k)\right|,$$

where $j = x, y, z$.

Table 3. Errors in the reorientation problem solution with one failed channel

Parameter	Error			
	normal operation	failure of channel x	failure of channel y	failure of channel z
Orientation, deg	0.0015	0.0021	0.0461	0.0289
Angular rate modulus $\|\boldsymbol{\omega}\|$, deg/s	less than $3.4 \cdot 10^{-7}$			

As can be seen from Table 3, the feasible accuracy of the solution of the terminal problem (7) is sufficient to ensure the fulfilment of the overwhelming majority of the target missions of scientific small spacecraft.

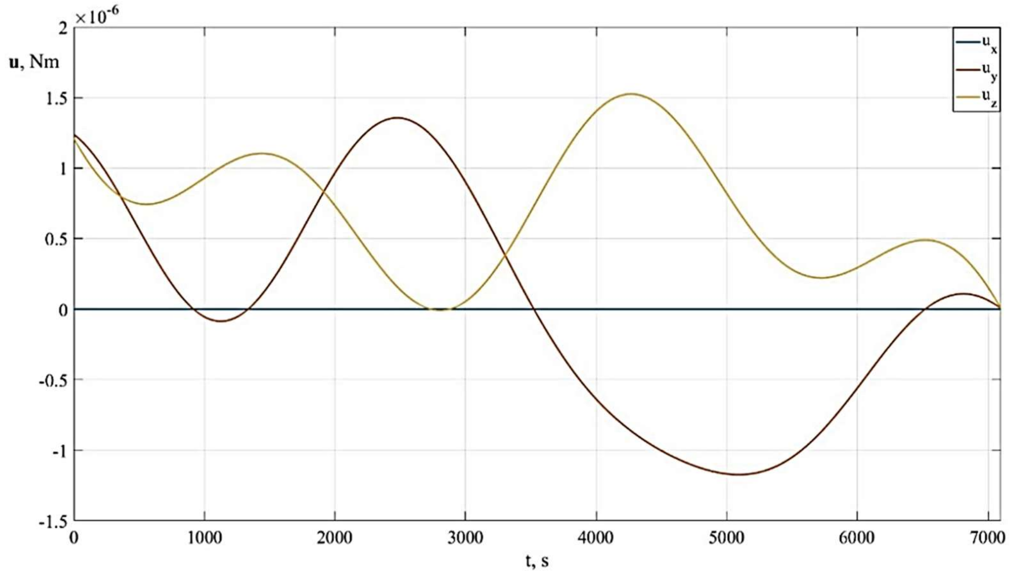

Fig. 6. Time dependence of control torques in the case of failure of the channel along the *Ox*-axis.

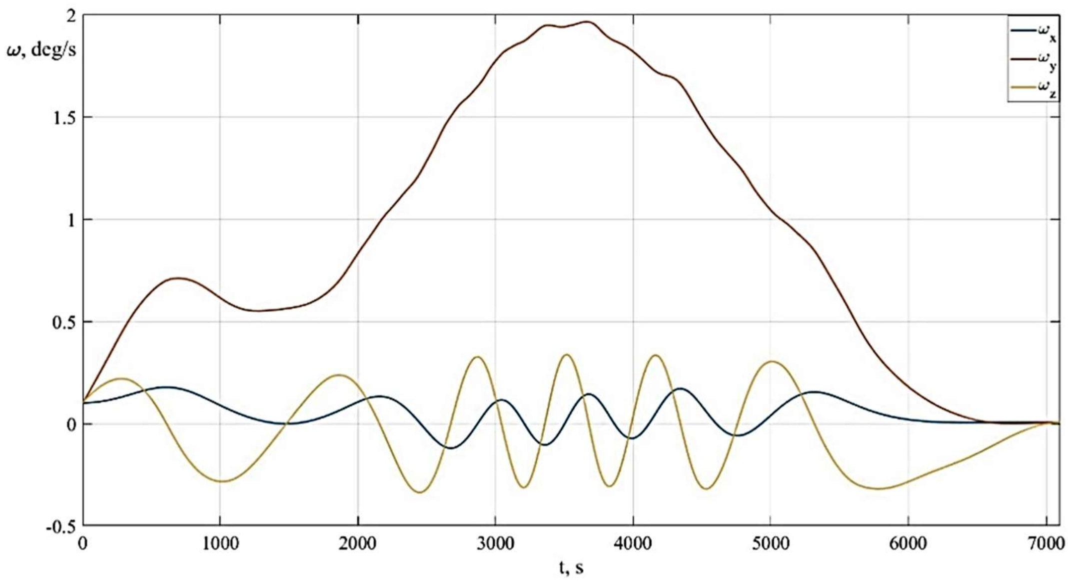

Fig. 7. Time dependence of angular rate components in the case of failure of the channel along the *Ox*-axis.

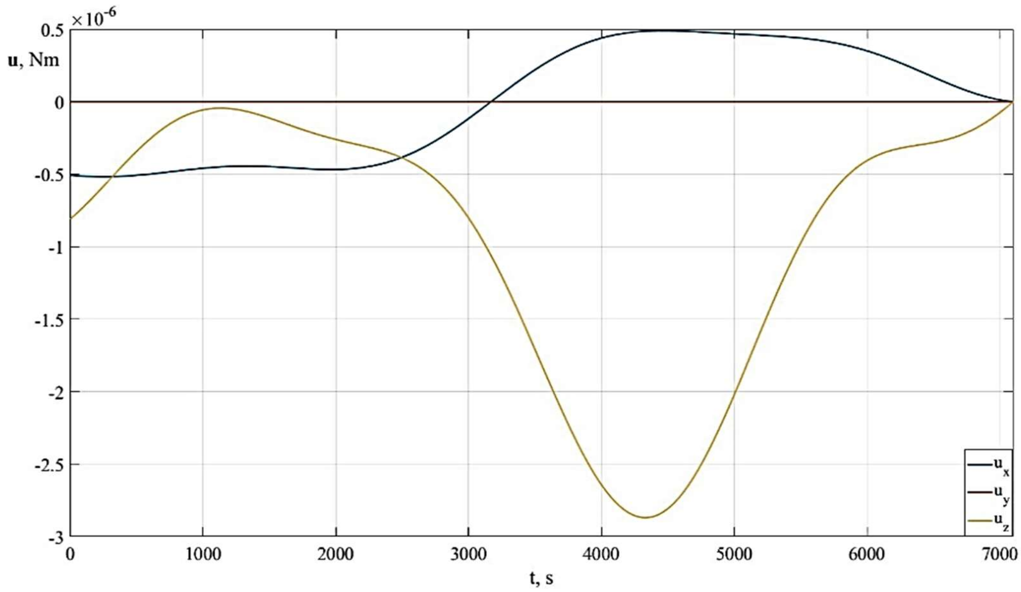

Fig. 8. Time dependence of control torques in the case of failure of the channel along the *Oy*-axis.

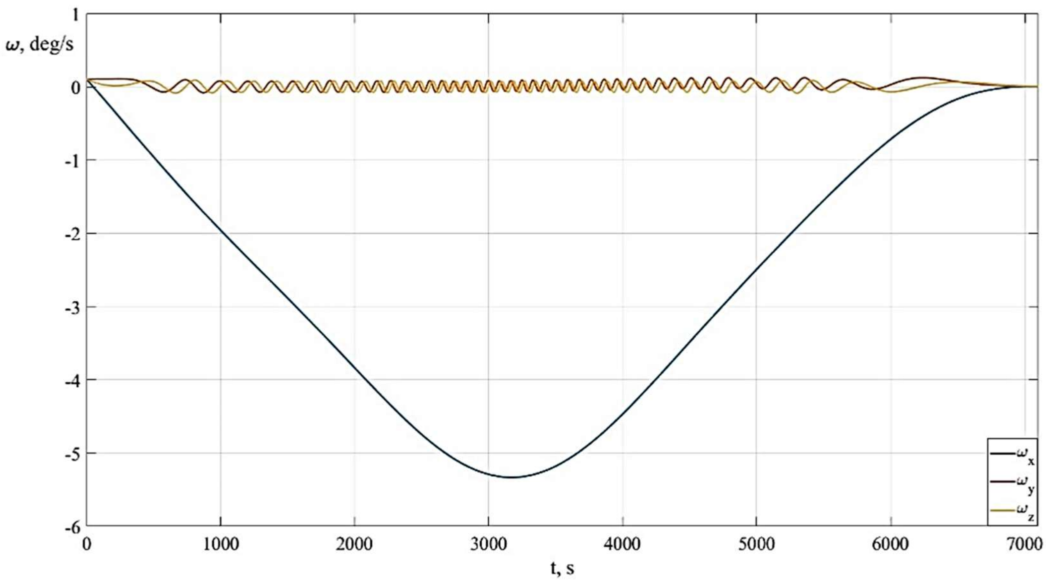

Fig. 9. Time dependence of angular rate components in the case of failure of the channel along the *Oy*-axis.

Figures 10–15 show the plots illustrating the solution of the SS reorientation problem (7) under the nominal program (8) with two failed control channels. Reorientation time t_k was 10 800 s.

As follows from Figs. 10, 12 and 14, the values of the control torque for various combinations of failures do not exceed $2 \cdot 10^{-6}$ Nm. Figures 11, 13 and 15 show that the values of the SS angular rate components during the reorientation process do not exceed 5 deg/s.

As can be seen from Table 4, the feasible accuracy of the solution of the terminal problem (7) is sufficient to ensure the fulfillment of the majority of target missions of scientific small spacecraft.

Table 4. Errors in the reorientation problem solution with two failed channels

Parameter	Error			
	Normal operation	Failure of channels *x* and *y*	Failure of channels *x* and *z*	Failure of channels *y* and *z*
Orientation, deg	0.0015	0.002	0.0557	0.183
Angular rate modulus $\|\boldsymbol{\omega}\|$, deg/s	less than $1.4 \cdot 10^{-5}$			

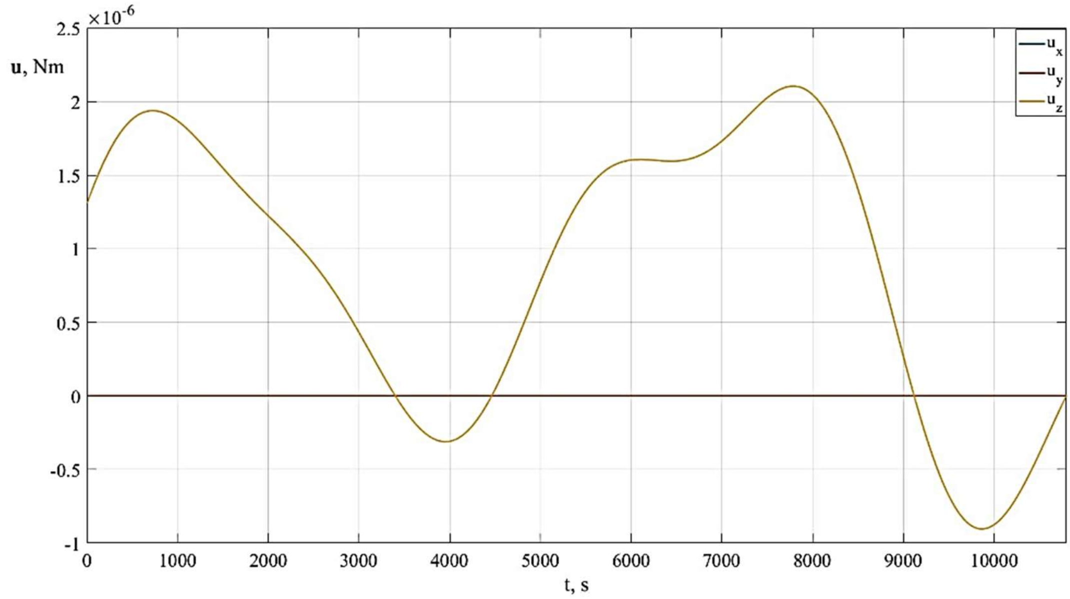

Fig. 10. Time dependence of the control torque in the case of failures of the channels along the *Ox*- and *Oy*-axes.

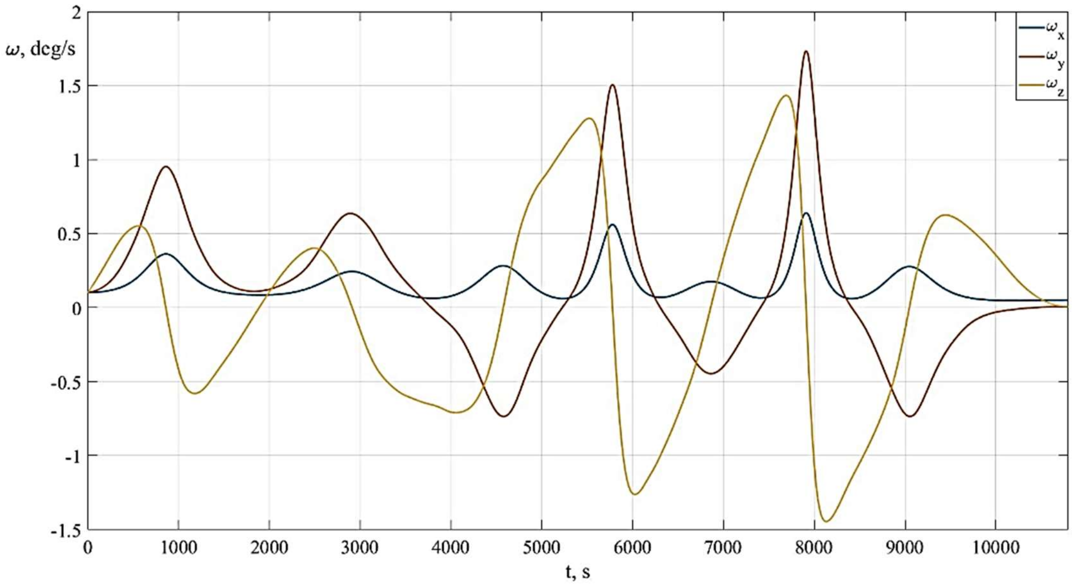

Fig. 11. Time dependence of the angular rate components in the case of failures of the channels along the *Ox*- and *Oy*-axes.

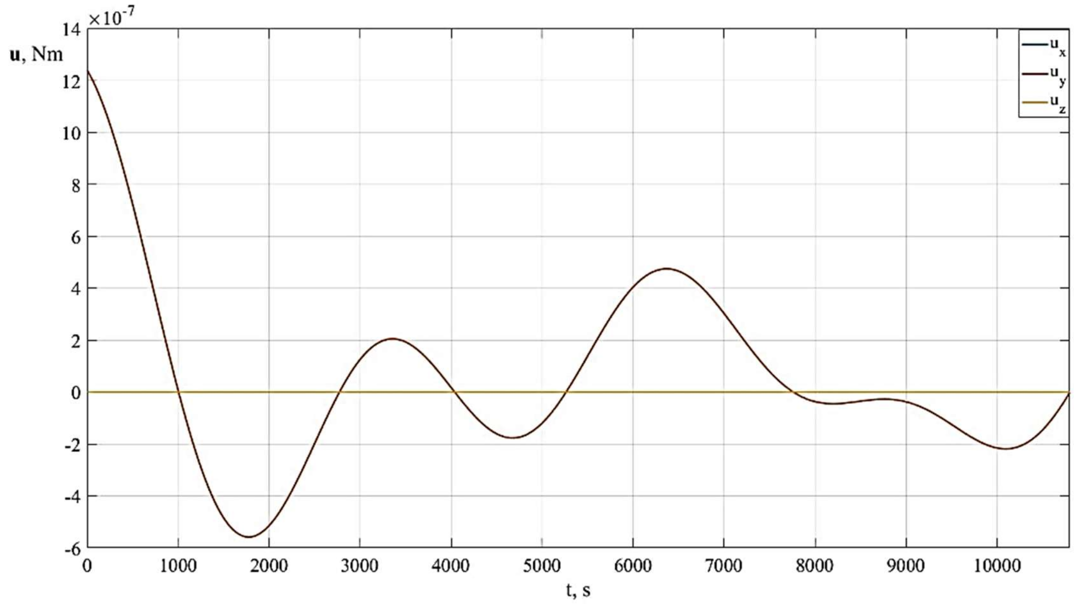

Fig. 12. Time dependence of the control torques in the case of failures of the channels along the *Ox*- and *Oz*-axes.

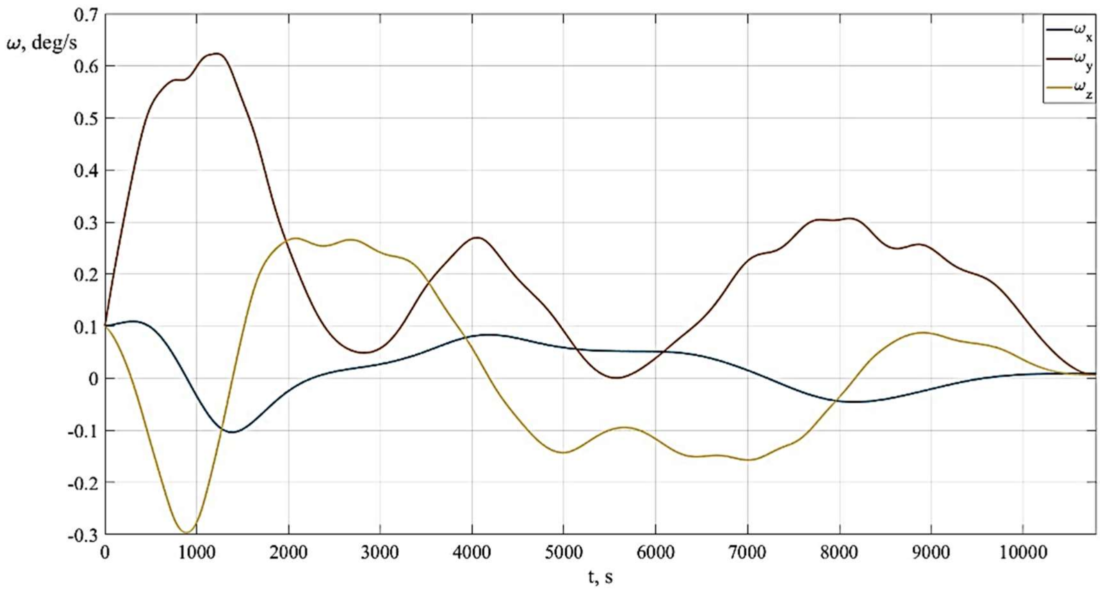

Fig. 13. Time dependence of angular rate components in the case of failures of the channels along the *Ox*- and *Oz*-axes.

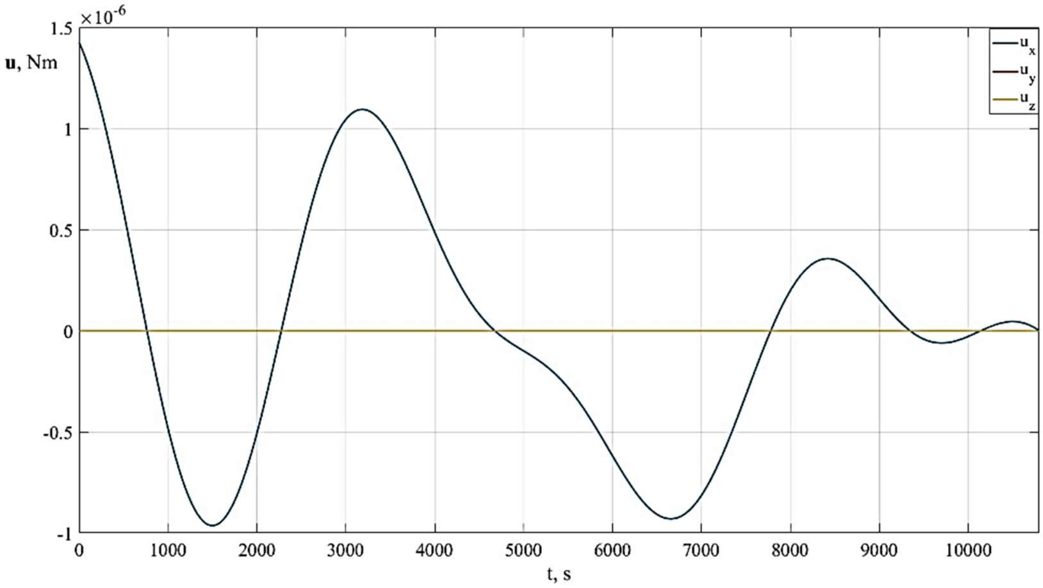

Fig. 14. Time dependence of the control torques in the case of failures of the channels along the *Ox*- and *Oz*-axes.

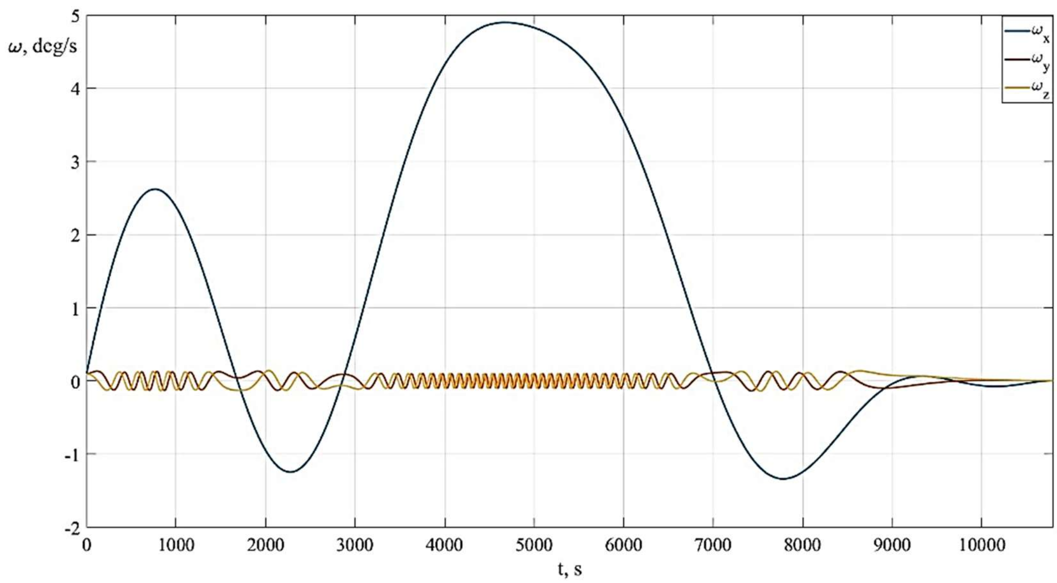

Fig. 15. Time dependence of the angular rate components in the case of failures of the channels along the *Oy*- and *Oz*-axes.

7. CONCLUSION

This paper describes the approach to designing an adaptive attitude control system for small spacecraft intended for science missions.

A digital twin has been proposed to detect failures of measuring equipment most frequently used by scientific small spacecraft. This makes it possible to predict measurements for a required point in time, which provides adaptation of the onboard mathematical model to the current state and operation conditions of the spacecraft. The methodology for diagnosing defects in measuring equipment is based on the comparison of the predicted results calculated in the digital twin with real measurements.

Failures of individual channels of actuators are compensated for with the use of the control algorithm with the structure in the form of even Fourier series. The solution to the problem is reduced to the calculation of 34 coefficients of the even Fourier series in the case that one channel has failed and 17, if two channels have failed. The coefficients were determined using a differential evolution algorithm. The time needed for reorientation in the case that one channel has failed is about 1.5 turns, and in the case of two failed channels, 2 turns. The magnitude of the control torque did not exceed $3 \cdot 10^{-6}$ Nm, which is feasible with the use of magnetic actuators that are most often installed in CubeSats.

The results obtained have practical significance; they may be useful for designers of small spacecraft, the type discussed in this study.

FUNDING

This work was supported by the Russian Science Foundation, project no. 23-67-10007. https://rscf.ru/project/23-67-10007/.

CONFLICT OF INTEREST

The author of this work declares that they have no conflicts of interest.

REFERENCES

1. Puig-Suari, J., Turner, C., and Twiggs, R.J., CubeSat: The development and launch support infrastructure for eighteen different satellite customers on one launch, *AIAA/USU Conference on Small Satellites*, 2001.
2. Bouwmeester, J. and Guo, J., Survey of worldwide pico- and nanosatellite missions, distributions and subsystem technology, *Acta Astronautica*, 2010, vol. 67, pp. 854–862.
3. Selva, D. and Krejci, D., A survey and assessment of the capabilities of Cubesats for Earth observation, *Acta Astronautica*, 2012, vol. 74, pp. 50–68.
4. Nanosats Database. https://www.nanosats.eu/. Accessed March 27, 2025.
5. Ivanov, D., Attitude motion and sensor bias estimation onboard the Sirius Sat-1 nanosatellite using magnetometer only, *Acta Astronautica*, 2021, vol. 188, pp. 295–307, https://doi.org/10.1016/j.actaastro.2021.07.038.
6. Carletta, S., Teofilatto, P., and Farissi, M.S., A magnetometer only attitude determination strategy for small satellites: Design of the algorithm and hardware-in the loop testing, *MDPI Aerospace*, 2020, vol. 7, no. 1, https://doi.org/10.3390/aerospace7010003.
7. Ivanov, D., Ovchinnikov, M., Ivlev, N., and Karpenko, S., Analytical study of microsatellite attitude determination algorithms, *Acta Astronautica*, 2015, vol. 116, pp. 339–348, https://doi.org/10.1016/j.actaastro.2015.07.001.
8. Markley, F.L. and Crassidis, J.L., *Fundamentals of Spacecraft Attitude Determination and Control*, *Springer*, 2014.
9. Yang, Y., *Spacecraft Modeling, Attitude Determination, and Control. Quaternion-based Approach*, Rockville, Maryland, USA: CRC Press, 2019. DOI:10.1201/9780429446580
10. Tkachev, S., Mashtakov, Y., Ivanov, D. Roldugin, D., and Ovchinnikov, M., Effect of reaction wheel imbalances on attitude and stabilization accuracy, *Aerospace*, 2021, 8, 252, https://doi.org/10.3390/aerospace8090252.
11. Roldugin, D., Okhitina, A., Monakhova, U., and Ovchinnikov, M., Comparison of Feedback Three-Axis Magnetic Attitude Control Strategies, *Aerospace*, 2023, 10, 975. https://doi.org/10.3390/aerospace10120975.
12. Saleh, J.H. and Castet, J.-F., *Spacecraft Reliability and Multi-state Failures: A Statistical Approach*, John Wiley & Sons, 2011, 224. DOI:10.1002/9781119994077
13. Tafazoli, M., A study of on-orbit spacecraft failures, *Acta Astronautica*, 2009, 64 (2–3), pp. 195–205, doi: 10.1016/j.actaastro.2008.07.019.
14. Wayer, J.K. Castet, J.-F., and Saleh, J.H., Spacecraft attitude control subsystem: Reliability, multi-state analyses, and comparative failure behavior in LEO and GEO, *Acta Astronautica*, 2013, vol. 85, pp. 83–92, doi: 10.1016/j.actaastro.2012.12.003.
15. Yin, S., Xiao, B., Ding, S. X., and Zhou, D., A review on recent development of spacecraft attitude fault tolerant control system, *IEEE Transactions on Industrial Electronics*, 2016, vol. 63, no. 5, pp. 3311–3320, doi: 10.1109/TIE.2016.2530789.
16. Tudoroiu, N. and Khorasani, K., Satellite fault diagnosis using a bank of interacting Kalman filters, *IEEE Transactions on Aerospace and Electronic Systems*, 2007, vol. 43, pp. 1334–1350, doi: 10.1109/TAES.2007.4441743.
17. Pirmoradi, F.N., Sassani, F., and de Silva, C.W., Fault detection and diagnosis in a spacecraft attitude determination system, *Acta Astronautica*, 2009, vol. 65, pp. 710–729, doi: 10.1016/j.actaastro.2009.03.002.

18. Henry, D., Fault diagnosis of microscope satellite thrusters using H-infinity/H- filters, *Journal of Guidance, Control, and Dynamics*, 2008., vol. 31, pp. 699–711, DOI: 10.2514/1.31003.
19. Gao, Z.F., Jiang, B., Shi, P., and Cheng, Y. H., Sensor fault estimation and compensation for microsatellite attitude control systems, *International Journal of Control Automation and Systems*, 2010, vol. 8, pp. 228–237, DOI: 10.1080/00207721.2010.517867.
20. Gao, C. Y., Zhao, Q., and Duan, G. R., Robust actuator fault diagnosis scheme for satellite attitude control systems, *Journal of the Franklin Institute*, 2013 vol. 350, pp. 2560–2580, doi: 10.1016/j.jfranklin.2013.02.021.
21. Zhang, J., Swain, A. K., and Nguang, S. K., Robust sensor fault estimation scheme for satellite attitude control systems, *Journal of the Franklin Institute*, 2013, vol. 350, pp. 2581–2604, doi: 10.1016/j.jfranklin.2013.06.010.
22. Pukdeboon, C., Zinober, A. S. I., and Thein, M. W. L., Quasi-continuous higher order sliding-mode controllers for spacecraft attitude tracking maneuvers, *IEEE Transactions on Industrial Electronics*, 2010, vol. 57, pp. 1436–1444, doi: 10.1109/TIE.2009.2030215.
23. Zhao, S.L. and Zhang, Y.C., SVM classifier-based fault diagnosis of the satellite attitude control system, *2008 International Conference on Intelligent Computation Technology and Automation*, Changsha, China, 2008, pp. 907–911.
24. Li, Z., Ma, L., and Khorasani, K., A dynamic neural network-based reaction wheel fault diagnosis for satellites, *International Joint Conference on Neural Networks*, Vancouver, BC, Canada, 2006, pp. 3714–3721.
25. Williamson, W.R., Speyer, J.L., Dang, V.T., and Sharp, J., Fault detection and isolation for deep space satellites, *AIAA Guidance, Navigation, and Control Conference and Exhibit*, Honolulu, USA, 2008, pp. 1570–1584.
26. Li, Z.Z., Liu, G.H., Zhang, R., and Zhu, Z.C., Fault detection, identification and reconstruction for gyroscope in satellite based on independent component analysis, *Acta Astronautica*, 2011, vol. 68, pp. 1015–1023, DOI: 10.1016/j.actaastro.2010.09.010.
27. Hu, D., Sarosh, A., and Dong, Y.F., A novel KFCM based fault diagnosis method for unknown faults in satellite reaction wheels, *ISA Transactions*, 2012, vol. 51, pp. 309–316, doi: 10.1016/j.isatra.2011.10.005.
28. Hu, Q., Shi, Y., and Shao, X., Adaptive fault-tolerant attitude control for satellite reorientation under input saturation, *Aerospace Science and Technology*, 2018, vol. 78, pp. 171–182. https://doi.org/10.1016/j.ast.2018.04.015.
29. Nasir, A. and Atkins, E.M., Fault tolerance for spacecraft attitude management, *AIAA Guidance, Navigation, and Control Conference*, Toronto, Canada, 2010.
30. Kruk, J.W., Class, B.F., Rovner, D., Westphal, J., Ake, T.B., Moos, H.W., Roberts, B., and Fisher, L., FUSE in-orbit attitude control with two reaction wheels and no gyroscopes, *The Conference on Future EUV/UV and Visible Space Astrophysics Missions and Instrumentation*, Bellingham, 2003.
31. Sweeting, M.N., Hashida, Y., Bean, N.P., Hodgart, M.S., and Steyn, H., CERISE microsatellite recovery from first detected collision in low Earth orbit, *Acta Astronautica*, 2004, vol. 55, pp. 139–147, doi: 10.1016/S0094-5765(03)00062-6.
32. GOST R 57700.37–2021. (Russian Federation State Standard R 577 00.37–2021) *Komp'yuternye modeli i modelirovanie. Tsifrovye dvoiniki izdelii. Obshchie polozheniya*. (Computer models and modeling. Digital twins of products. General provisions).
33. Krylov, V.I., *Osnovy teorii dvizheniya ISZ* (Chast' 2: *Vozmushchennoe dvizhenie*) (Fundamentals of the Theory of Artificial Satellite Motion (Part 2: Disturbed Motion): Textbook, Moscow: MIIGAiK. 2016.
34. Belokonov, I.V., Timbai, I.A., and Nikolaev, P.N., Analysis and Synthesis of Motion of Aerodynamically Stabilized Nanosatellites of the CubeSat Design, *Gyroscopy and Navigation*, 2018, vol. 9, no. 4, pp. 284–297. DOI: 10.1134/S2075108718040028
35. Picone, J.M., Hedin, A.E., Drob, D.P., and Aikin, A.C., NRLMSISE-00 empirical model of the atmosphere: Statistical comparisons and scientific issues, *Journal of Geophysical Research Atmospheres*, 2002, 107 (A12), DOI:10.1029/2002JA009430.
36. Sinpetru, L.A., Crisp, N.H., Mostaza-Prieto, D., Livadiotti, S., and Roberts, P.C.E., ADBSat: Methodology of a novel panel method tool for aerodynamic analysis of satellites, *Preprint submitted to Computer Physics Communications*, 2021, https://doi.org/10.1016/j.cpc.2022.108326.
37. Bird, G.A., *Molecular Gas Dynamics and the Direct Simulation of Gas Flows.* Oxford: Clarendon Press, 1994.
38. Nikolaev, P.N., Espinoza V.A.S., Shcherbakov, M.S., and Sobolev, D.D., Calibration of onboard magnetometers of the attitude control system of the SamSat-ION university nanosatellite. *Gyroscopy and Navigation*, 2023, 14, pp. 259–266. https://doi.org/10.1134/S2075108723030069.
39. Syed, Z.F., Aggarwal, P., Goodall, C., Niu, X., and El-Sheimy, N., A new multi-position calibration method for MEMS inertial navigation systems, *Measurement Science and Technology*, 2007 May 15; 18(7):1897, doi 10.1088/0957-0233/18/7/016.
40. Hajiyev, C. and Soken, H.E., *Fault Tolerant Attitude Estimation for Small Satellites* (1st ed.), *CRC Press*, 2020. https://doi.org/10.1201/9781351248839.
41. Zheng, T., Zheng, F., Rui, X., Ji, X., A Precise Algorithm for Computing Sun Position on a Satellite, *Journal Aerospace Technology and Management*, 2019, vol. 11, doi: 10.5028/jatm.v11.1048.
42. Hajiyev, C., Orbital Calibration of Microsatellite Magnetometers Using a Linear Kalman Filter, *Measurement Techniques*, 2015, 58, 1037–1043, https://doi.org/10.1007/s11018-015-0838-4.
43. Soken, H.E. and Hajiyev, C., UKF based in-flight calibration of magnetometers and rate gyros for pico satellite attitude determination, *Asian Journal of Control*, 2012, 14, no. 3, 707–715, doi: 10.1002/asjc.368.
44. Belokonov, I.V. and Lomaka, I.A., In-flight calibration of nanosatellites inertia tensor: The algorithm and requirements for on-board sensors, *Proceedings of the International Astronautical Congress, IAC,* 2018.
45. Kramlikh, A.V., Nikolaev, P.N., and Rylko, D.V., Onboard two-step attitude determination algorithm for a SamSat-ION nanosatellite. *Gyroscopy and Navigation,* 2023*,* vol. 14, pp. 138–153.

https://doi.org/10.1134/S2075108723020050
46. Cilden-Guler, D. and Hajiyev, C., SVD-Aided EKF for Nanosatellite Attitude Estimation Based on Kinematic and Dynamic Relations, *Gyroscopy and Navigation*, 2023, vol. 14, pp. 366–379.
47. Searcy, J.D. and Pernicka, H.J., Magnetometer-only attitude determination using novel two-step Kalman filter approach, *Journal of Guidance Control and Dynamics*, 2012, vol. 35, pp. 1639–1701.
48. Belokonov, I.V. and Kramlikh, Methodology for recovery of the spacecraft attitude by combining magnetometric and radio navigation measurements, *Vestnik Samarskogo gosudarstvennogo aerokosmicheskogo universiteta imeni akademika S.P. Koroleva*, 2007, no. 1 (12), pp. 22–30.
49. Belokonov, I.V., Kramlikh, A.V., Lomaka, I.A., and Nikolaev, P.N., Reconstruction of a Spacecraft's Attitude Motion Using the Data on the Current Collected from Solar Panels, *Journal of Computer and Systems Sciences International*, 2019, vol. 58, issue 2, pp. 286–296. doi:10.1134/S1064230719020047
50. Belokonov, I.V. and Lomaka, I.A., Postflight Recovery of the Rotational Motion of a Small Space Vehicle from Solar Sensor Information, *Journal of Computer and Systems Sciences International*, 2023, vol. 62, no. 2, pp. 214–224.
51. Elisov, N.A., Kramlikh, A.V., Lomaka, I.A., and Avariaskin, D.P., An attitude control by the functional series in the problem of nanosatellite reorientation, *Aerospace Science and Technology*, 2023, vol. 132. doi: 10.1016/j.ast.2022.108038.
52. Elisov, N.A., Kramlikh, A.V., and Lomaka, I.A., Synthesis of nominal trajectories of reorientations of small spacecraft in case of failure of one control channel, *Mekhatronika, Avtomatizatsiya, Upravlenie,* 2023, 24 (11), pp. 608–615. https://doi.org/10.17587/mau.24.608-615.
53. Storn, R. and Price, K., Differential Evolution - A Simple and Efficient Heuristic for Global Optimization over Continuous Spaces, *Journal of Global Optimization*, 1997, no. 11, pp. 341–359.
54. Hall, D., Spacecraft Attitude Dynamics and Control, *Virginia Polytechnic Institute and State University: Blacksburg*, 2003.